DNM2 levels normalization improves muscle phenotypes of a novel mouse model for moderate centronuclear myopathy

Juliana de Carvalho Neves, Foteini Moschovaki-Filippidou, Johann Böhm, Jocelyn Laporte

Molecular Therapy
Nucleic Acids
Original Article

DNM2 levels normalization improves muscle phenotypes of a novel mouse model for moderate centronuclear myopathy

Juliana de Carvalho Neves,[1] Foteini Moschovaki-Filippidou,[1] Johann Böhm,[1] and Jocelyn Laporte[1]

[1]Institut de Génétique et de Biologie Moléculaire et Cellulaire (IGBMC), CNRS UMR7104, INSERM U1258, 1 rue Laurent Fries, 67404 Illkirch Cedex, France

Dynamin 2 (DNM2) is a ubiquitously expressed GTPase regulating membrane trafficking and cytoskeleton dynamics. Heterozygous dominant mutations in *DNM2* cause centronuclear myopathy (CNM), associated with muscle weakness and atrophy and histopathological hallmarks as fiber hypotrophy and organelles mis-position. Different severities range from the severe neonatal onset form to the moderate form with childhood onset and to the mild adult onset form. No therapy is approved for CNM. Here we aimed to validate and rescue a mouse model for the moderate form of DNM2-CNM harboring the common *DNM2* R369W missense mutation. *Dnm2*$^{R369W/+}$ mice presented with increased DNM2 protein level in muscle and moderate CNM-like phenotypes with force deficit, muscle and fiber hypotrophy, impaired mTOR signaling, and progressive mitochondria and nuclei mis-position with age. Molecular analyses revealed a fiber type switch toward oxidative metabolism correlating with decreased force and alteration of mitophagy markers paralleling mitochondria structural defects. Normalization of DNM2 levels through intramuscular injection of AAV-sh*Dnm2* targeting *Dnm2* mRNA significantly improved histopathology and muscle and myofiber hypotrophy. These results showed that the *Dnm2*$^{R369W/+}$ mouse is a faithful model for the moderate form of DNM2-CNM and revealed that DNM2 normalization after a short 4-week treatment is sufficient to improve the CNM phenotypes.

INTRODUCTION

Dynamin 2 (DNM2) is a large mechanochemical GTPase that is implicated in several cellular processes including endocytosis, apoptosis, cytokinesis, phagocytosis, and cell migration,[1–3] being engaged in cell membrane trafficking and cytoskeleton remodeling.[4] DNM2 is composed of several protein domains: the N-terminal GTPase domain, the middle domain (MID) and GTPase effector domain forming a stalk responsible for protein oligomerization, a pleckstrin homology domain (PH) binding membrane, and the C-terminal proline-arginine-rich domain (PRD) binding to effector proteins with an Src homology (SH3) domain (Figure 1A).[5–9] *DNM2* is ubiquitously expressed and has different isoforms, either containing exon 10a/b in mutually exclusive splicing or including the alternative spliced exons 12b and 13b.[10,11] Exon12b inclusion is specific to muscles and increases during development, while human and mouse adult muscles express this muscle-specific and the ubiquitous DNM2 isoforms equally.[11]

Heterozygous mutations in *DNM2* gene are one of the main causes of centronuclear myopathy (CNM), a subclass of congenital myopathies with slowly progressive muscle weakness affecting children to adults of both sexes and diverge ethnic origin (ADCNM, MIM: 160150).[12] These mutations act in a dominant inheritance pattern and are believed to be gain of function. Indeed, *in vitro* experiments with mutated DNM2 revealed increased stability of oligomers and GTPase activity, independently of lipid binding,[13–15] and overexpression of wild-type (WT) DNM2 triggers a CNM-like phenotype in mice.[16,17] Patients carrying *DNM2* mutations present a broad variability in the symptoms severity and age of onset, from a severe neonatal form to a moderate (intermediate) severity and to a mild form with adult onset.[12,18–24] In early onset severe cases, the symptoms include generalized muscle weakness, hypotonia, facial weakness, ophthalmoplegia, ptosis, and breathing difficulties.[20] Moderate cases have delayed motor development milestones during childhood, difficulties for walking, running, or climbing stairs, while mild cases display a diffuse and slowly progressive myopathy from 20 to 40 years. As histopathological hallmarks, muscle biopsies show a predominance of oxidative fibers, fiber size heterogeneity, and central accumulation of oxidative activity and nuclei.[25]

The CNM pathomechanism is only partially understood. Analysis of zebrafish models and mice knockin for a severe (S619L) or mild (R465W) mutation reported defects in neuromuscular junctions, organelle positioning, calcium handling, and autophagy.[26–30] No therapies are currently available to treat CNM patients, but therapeutic proof of concepts have been successful in pre-clinical models. Acetylcholine esterase inhibitors and DNM2 downregulation were proposed for DNM2-CNM. Acetylcholine esterase inhibitors target the alteration of neuromuscular junctions.[31,32] DNM2 downregulation, with antisense oligonucleotides or shRNA, rescued the locomotor, histological, and force defects of *Dnm2*$^{S619L/+}$ and *Dnm2*$^{R465W/+}$ mice,

Received 6 November 2022; accepted 11 July 2023;
https://doi.org/10.1016/j.omtn.2023.07.003.

Correspondence: Jocelyn Laporte, Institut de Génétique et de Biologie Moléculaire et Cellulaire (IGBMC), 67400 Illkirch Cedex, France.
E-mail: jocelyn@igbmc.fr

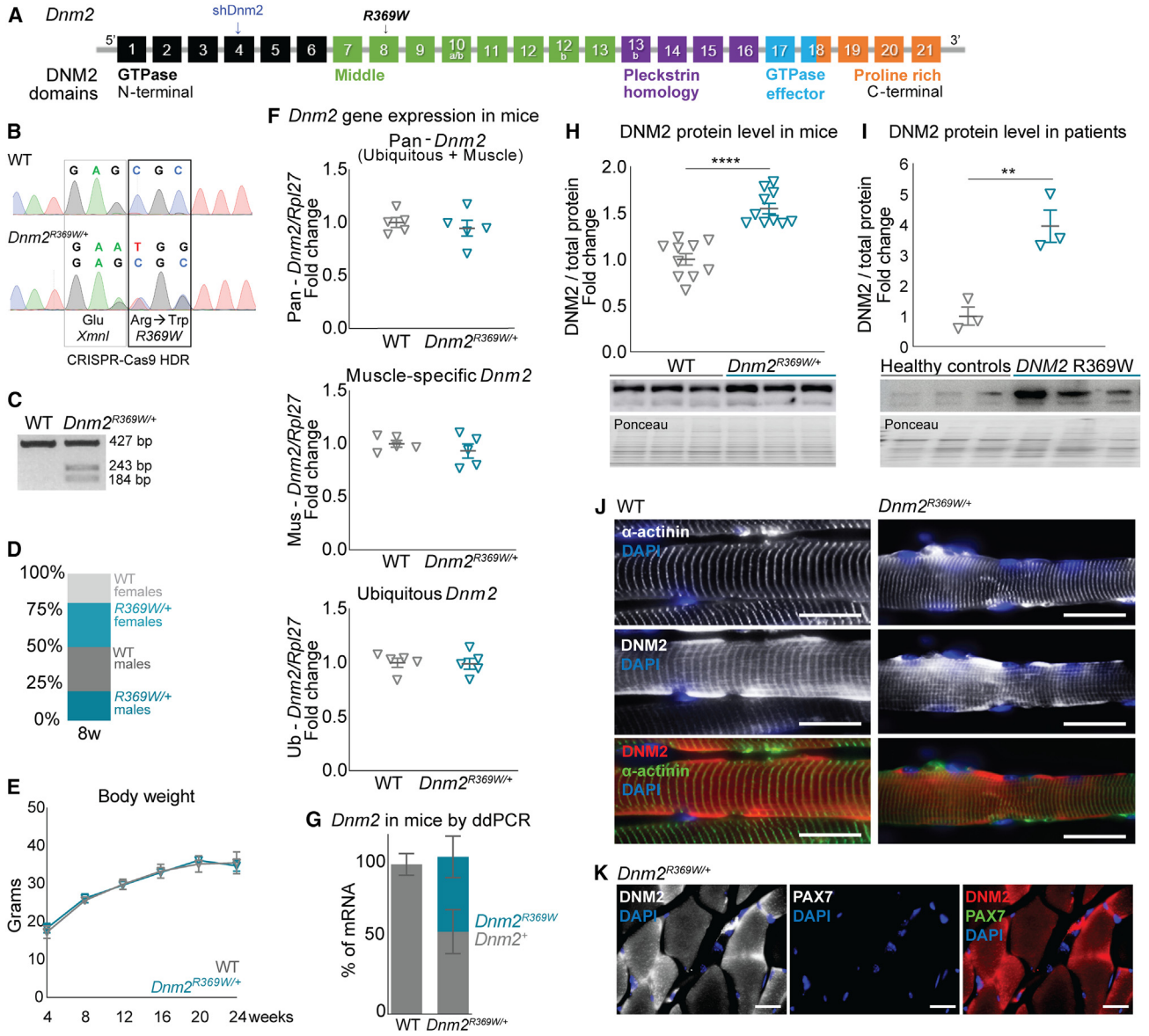

Figure 1. Creation and validation of *Dnm2*$^{R369W/+}$ mice

(A) *Dnm2* exonic representation and the respective DNM2 protein domains: GTPase, middle, pleckstrin homology, GTPase effector, and proline rich. The exons 10a, 10b, 12b, and 13b can be alternatively spliced. *DNM2* R369W mutation was knocked in by CRISPR-Cas9 in the exon 8. The sh*Dnm2* that was used in this study to downregulate DNM2 targets exon 4. (B) Chromatopherograms of WT and *Dnm2*$^{R369W/+}$ mice, which present a GAG>GAA synonym mutation for genotyping purpose and the Arg>Trp R369W CNM mutation (CGC to TGG). (C) Example of genotyping with amplicons of different molecular weights: the WT allele as a 427-bp band and the *Dnm2*^{R369W} mutated alleles as two bands of 243 bp and a 184 bp, generated by the cleavage of the Glu GAA site by the restriction enzyme *XmnI*. (D) Proportion of genotypes in the mouse offspring at 8 weeks of life (n = 30 mice). Chi-square test, p = 0.75. (E) Body weight (n = 10 up to 8 weeks, n = 5 from 12 to 24 weeks). (F) *Dnm2* mRNA expression of pan (ubiquitous + muscle-specific), muscle-specific (exon 12B), and ubiquitous and *Dnm2* isoforms (n = 5). (G) Absolute quantification of mutated and WT forms of *Dnm2* by ddPCR. Two-way ANOVA for allelic source of variation: p = 0.0002. (H) DNM2 protein expression in *Dnm2*$^{R369W/+}$ mice (n = 10, ~110, and 120 kDa) or (I) patients harboring the CNM *DNM2* R369W mutation (n = 3). (J) Immunofluorescence of longitudinal and (K) transversal muscle sections for DNM2 localization with the Z line marker α-actinin and the satellite cell marker PAX7 (n = 3). Samples from mice at 8 weeks old. Mean ± SEM, unpaired t test, **p < 0.01: CNM *DNM2*$^{R369W/+}$ differs from healthy controls, ****p < 0.0001: *Dnm2*$^{R369W/+}$ differs from WT. Bars represent 20 μm.

models for the severe and mild DNM2-CNM respectively.[30,33] Specific reduction of the *Dnm2* mutated allele with siRNA also improved the phenotypes of the *Dnm2*$^{R465W/+}$ mice.[34]

A main bottleneck in this field is whether DNM2 downregulation would be therapeutic on different severity forms and mutations in *DNM2*.[35] Here, we first created a mammalian model for the moderate

DNM2-CNM form and tested DNM2 downregulation with *in vivo* expression of a specific shRNA against *Dnm2*. We selected the R369W *DNM2* mutation, as among the most common mutation linked to moderate cases with age of onset ranging from childhood to adulthood and with variable symptoms that may include muscle weakness (either proximal, distal, or diffuse), facial weakness, ophthalmologic involvement, hyperlordosis, walking difficulties, and impairment of tendon reflexes at different intensities.[20] We found the *Dnm2*$^{R369W/+}$ mouse is a faithful model for the moderate CNM form and presents increased DNM2 level and alteration of metabolic and mitochondria functions in addition to a CNM histopathology and muscle involvement. DNM2 normalization upon a single injection of adeno-associated virus (AAV)-sh*Dnm2* was sufficient to improve these alterations.

RESULTS

Creation and initial characterization of the *Dnm2*$^{R369W/+}$ mouse for moderate DNM2-CNM

The *DNM2* R369W mutation in the middle domain was introduced in mice using CRISPR-Cas9. Three point mutations were created in the exon 8 of the *Dnm2* gene: the CGC>TGG mutations resulting in the substitution of an arginine by a tryptophan and a flanking synonymous mutation GAG>GAA (Glu) for genotyping purposes (Figures 1A and 1B). The presence of these heterozygous mutations was confirmed by genotyping and Sanger sequencing (Figures 1B and 1C).

Dnm2$^{R369W/+}$ males and females were successfully generated and fertile. They were bred with WT mice, producing offspring following Mendelian proportion (Figure 1D). *Dnm2*$^{R369W/+}$ mice were studied at different ages from 3 to 24 weeks to assess the clinical, histological, and force phenotypes. No postnatal deaths were observed up to 24 weeks of life. At all ages studied, *Dnm2*$^{R369W/+}$ mice presented no clear physical signs associated with myopathy such as kyphosis, breathing or walking difficulties, nor body weight loss (Figure 1E), albeit unilateral ptosis was observed in 2% of them. We observed three males of each genotype up to their natural death, and their lifespan was around 1 year and 8 months, regardless of the genotype.

We next assessed if the mutation in *Dnm2* gene impacts the corresponding mRNA and protein expression. No alteration was observed in gene expression of pan-*Dnm2*, muscle-specific, nor ubiquitous isoforms in the TA (tibialis anterior) muscles of *Dnm2*$^{R369W/+}$ mice at 8 weeks of age (Figure 1F), and the expression of the mutated and WT forms of *Dnm2* mRNA each accounted for about 50%, as verified by reverse transcription droplet digital PCR (RT-ddPCR, Figure 1G). However, DNM2 protein level was significantly increased by 50% in the *Dnm2*$^{R369W/+}$ mouse model (Figure 1H), mimicking the upregulation found in the muscles of CNM patients carrying the *DNM2* R369W mutation versus healthy controls (Figure 1I).

Immunofluorescence in longitudinal muscle sections indicated that DNM2 was mainly colocalized with α-actinin, a Z line marker (Figure 1J). DNM2 was also present in PAX7-negative cells adjacent to muscle fibers and at the periphery of the fiber in transverse sections (Figure 1K). All these results indicate that the R369W mutation has no strong effect on protein localization but causes DNM2 increased levels in muscles of the *Dnm2*$^{R369W/+}$ mouse.

Muscle weakness in *Dnm2*$^{R369W/+}$ mice

We next submitted *Dnm2*$^{R369W/+}$ mice to force grip and four limbs hanging tests from 3 to 24 weeks of age and verified the contractile properties of TA muscles at 8 weeks of age. *Dnm2*$^{R369W/+}$ mice had the same performance in the grip and hanging tests as the control WT mice; however, they may have compensated a lack of distal force by relying on the forelimbs to keep holding the grid (Figures 2A–2C and Video S1). Thus, the contractile properties were measured based on the force response by isolated TA muscles after sciatic nerve stimulation to simulate the maximum force production (stimulations at ascendant frequencies) or the susceptibility to fatigue (repeated 40-Hz stimulations). *Dnm2*$^{R369W/+}$ performed as WT mice in the simulation of susceptibility to fatigue (Figure 2D). However, the experiment of force production revealed decreased submaximal force ($\geq$50 Hz) and decreased maximum absolute and specific force (at 100 Hz), supporting that *Dnm2*$^{R369W/+}$ mice present force deficit (Figures 2E and 2F).

Dnm2$^{R369W/+}$ muscle recapitulates CNM histological hallmarks

Alteration in fiber diameter is among the histological hallmarks of CNM, also including centralized nuclei and abnormal oxidative staining.[25] At 8 weeks of age, the TA muscles from *Dnm2*$^{R369W/+}$ mice were hypotrophic compared to WT, as indicated by the reduction of 10% in the ratio of TA muscle weight normalized to body weight (Figure 3A). Transverse sections of soleus muscles stained with hematoxylin and eosin (H&E) did not present obvious alterations (Figure S1), while TA muscles had fibers with smaller diameter (<40 μm), a decreased number of large fibers (>40 μm), and nuclei correctly placed at the periphery of the fibers (Figures 3B–3D). The succinate dehydrogenase (SDH) staining presented central and necklace-like accumulation of oxidative activity in 9.6% and 2.17% of the fibers, respectively, while these defects were never noted in WT (Figure 3E). In the soleus muscles, central staining was found in 3.23%, while absent in WT (Figure S1). Together, the impaired histology, the deficits in muscle force, and DNM2 overexpression validate the *Dnm2*$^{R369W/+}$ mice as a faithful CNM mouse model.

Dnm2$^{R369W/+}$ mice were also analyzed at 24 weeks old to assess a potential progression of the muscle disease. The gastrocnemius (GA) and TA muscles from mutated mice presented a reduction in the mass when comparing 24 and 8 weeks of life. In the case of the TA muscles, the ratio of muscle per body weight decreased by 22% (Figure 3A), and the number of internalized nuclei was five times higher compared to controls (Figures 3B and 3C). Although the SDH abnormal staining remained at the same levels, the profile of accumulation changed from predominantly centralized (9.6%) at 8 weeks to a half-half mix of centralized SDH staining and necklace-like staining (7.7% and 7.2% respectively) at 24 weeks (Figure 3E). Nearly 1% of the fibers evolved to a radial disposition of SDH staining (aspect of

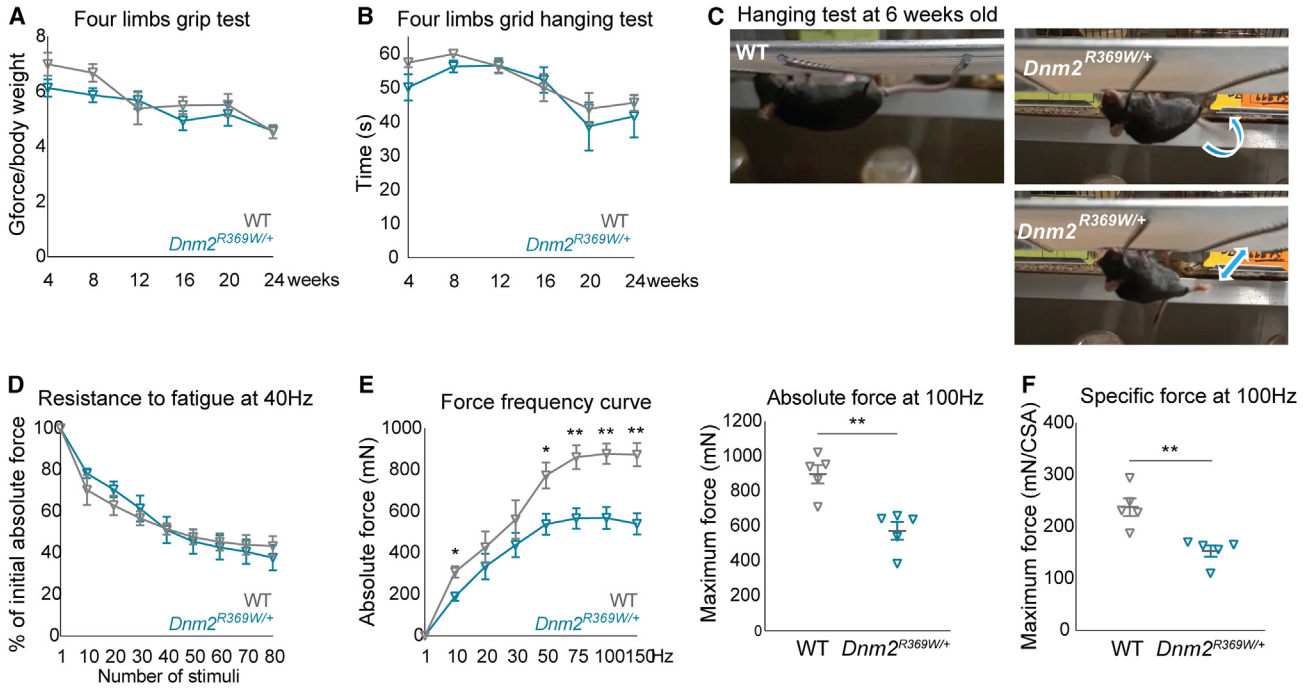

Figure 2. Muscle strength tests and deficits in the contractile properties

(A) Four limbs grip test and (B) hanging test (n = 10 up to 8 weeks, n = 5 from 12 to 24 weeks). (C) Representative rotatory movements of the tail and forelimbs during the hanging test at 6 weeks of age (see Video S1). (D) TA muscle resistance to fatigue after sciatic nerve stimulations at 40 Hz. (E) Submaximal and maximum absolute force outputs and (F) maximum absolute force and (G) maximum specific force (n = 5 at 8 weeks old). The maximum force was calculated at 100 Hz. The specific force is expressed as the ratio of the force produced (mN) by the cross-sectional area of the muscle analyzed (CSA = muscle weight (mg)/muscle length (mm) x muscle density 1.06 mg/mm^3). Mean ± SEM, Mann-Whitney or unpaired t test, *p < 0.05 and **p < 0.01: *Dnm2*$^{R369W/+}$ differs from WT.

"spoke of wheels"), a typical pattern in CNM patients. These results suggest that the TA muscle phenotype of *Dnm2*$^{R369W/+}$ mice progressed from 8 to 24 weeks old.

Muscle fiber disorganization underlies the muscle weakness

To assess the cause of the muscle weakness, we investigated further the fiber ultrastructural organization. In accordance with the result of abnormal SDH oxidative staining, structural mitochondrial defects were found in electron microscopy (n = 2, Figure 4A). *Dnm2*$^{R369W/+}$ muscles presented with a subgroup of mitochondria with normal shape and size but also enlarged mitochondria sometimes with disrupted cristae. In corroboration, we found that prohibitin, a marker of inner mitochondrial membrane and a mitophagy receptor,[36] was downregulated in *Dnm2*$^{R369W/+}$ mice (Figure 4B). No mitochondrial fragmentation nor autophagic vacuoles were observed in electron microscopy.

One of the main mitophagy pathways is mediated by PTEN-induced putative kinase 1 (PINK1)/Parkin 2 (PARK2)[37–39] and regulated by *Sirt1*.[40] We found that the mRNA levels of *Sirt1* were half of the values found for the WTs (Figure 4C) and, although *Pink1* and *Park2* mRNA expression did not differ between genotypes (values normalized to the WTs = 1: *Pink1* 0.97 SEM ± 0.07 p = 0.11, *Park2* 1.10 ± 0.03 SEM p = 0.23, n = 5 each genotype), the E3 ubiquitin ligase PARK2 was found increased (Figure 4D). The mTOR pathway is related with mitochondrial homeostasis and implicated in mitochondrial function[41] and autophagy suppression.[42] We investigated the activity of the mTOR pathway through the phosphorylation level of S6K, a major downstream target. The phosphorylation of S6K was indicated by the 2.5-fold higher ratio of phosphorylated per total form in *Dnm2*$^{R369W/+}$ (Figure 4E). Altogether, these results suggest that mitophagy is impaired in the TA muscles of *Dnm2*$^{R369W/+}$ mice.

The electron microscopy also revealed a combination of triads with normal aspect and others with shape defects in the *Dnm2*$^{R369W/+}$ muscles, as enlargement of the T-tubule (Figure 4A). Triads are essential membrane structures for excitation-contraction coupling and are composed of two terminal cisternae from the sarcoplasmic reticulum and a central T-tubule.[43] To evaluate further the T-tubules, immunofluorescence experiments were performed for dihydropyridine receptor (DHPR), a voltage-gated calcium channel found at the T-tubule,[44,45] and for amphiphysin 2 (BIN1), a protein implicated in T-tubules formation.[46,47] While DHPR and BIN1 localization was not obviously altered (Figure 4F), correlating with the normal localization of triad seen by electron microscopy, BIN1 protein was found 20% overexpressed in TA muscles of *Dnm2*$^{R369W/+}$ mice at 8 weeks, confirming alteration of T-tubule maintenance as a pathomechanism (Figure 4G).

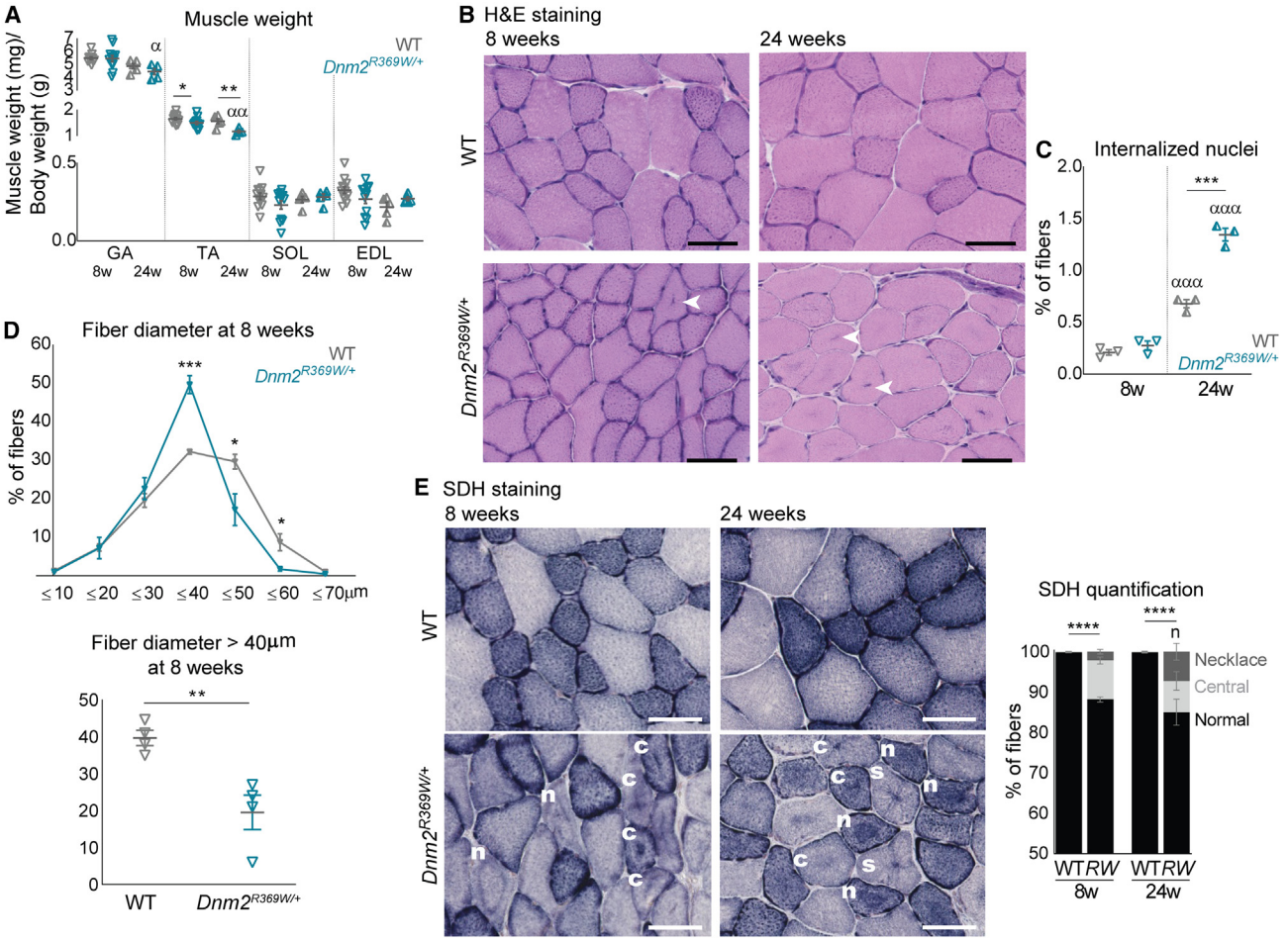

Figure 3. Muscle hypotrophy and histological hallmarks of centronuclear myopathy

(A) Ratio of hindlimbs muscle weight per body weight at 8 and 24 weeks of age (8w and 24w). GA, gastrocnemius; TA, tibialis anterior; SOL, soleus; EDL, extensor digitorum longus. Analyses of muscle sections at 8 weeks old, with 2 mm^2 analyzed per muscle. The TA muscles sections stained with hematoxylin and eosin were used for determining (B) the general histological aspect (n = 5), (C) the percentage of fibers presenting internalized nuclei (n = 3), and (D) the fiber diameter (n = 4). (E) SDH oxidative staining showed abnormal central accumulation (c), necklace fibers (n), or spokes of wheels aspect (s) (n = 3). Mean ± SEM, Mann-Whitney or unpaired t test, *p < 0.05, **p < 0.01, ***p < 0.001, and ****p < 0.0001: *Dnm2*$^{R369W/+}$ differs from WT at the same age; α p < 0.05, αα p < 0.01, and ααα p < 0.001: *Dnm2*$^{R369W/+}$ at 8 weeks differs from *Dnm2*$^{R369W/+}$ at 24 weeks; n p < 0.05: *Dnm2*$^{R369W/+}$ necklace fibers at 8 weeks differs from *Dnm2*$^{R369W/+}$ 24 weeks. Bars represent 50 µm.

Desmin is a protein found at the Z line that is pivotal for maintaining the muscle structure and function[48] and the correct mitochondrial and nuclei positioning.[49] DNM2-CNM patients accumulate desmin in the center of the fibers.[25] Accordingly, 6.7% of the *Dnm2*$^{R369W/+}$ fibers were positive for internal desmin accumulation at 8 weeks of age versus 0.38% in WT controls (n = 3, p = 0.015) (Figure 4H). These results indicate that *Dnm2*$^{R369W/+}$ mice present disorganization of the muscle fiber structure and accumulation of muscle-specific proteins, similarly to DNM2-CNM patients.

Dnm2$^{R369W/+}$ muscles present alterations in muscle fiber metabolism

Alteration in fiber type specification toward an increase in slow-twitch fibers with high oxidative capacity (i.e., type I) is a hallmark of CNM and more generally congenital myopathies.[25] However, a previous study conducted in *Dnm2*$^{R465W/+}$ mice showed WT fiber type composition may be linked to the mild-form muscle phenotypes of this model.[50] Here, we estimated the myofibers profile through mRNA expression of myosin isoforms and immunofluorescent co-labeling of myosins type I (MYH7), IIa (MYH2), and IIb (MYH4) in the TA muscles of *Dnm2*$^{R369W/+}$ mice at 8 weeks of age. We focused on the TA muscles as they were the most affected of the muscles tested (Figure 5A) and are fast-twitch muscles with no slow type I fibers and very low intermediate type IIa fibers,[51,52] where a slower specification would be easy to highlight. Fast fibers positive for type IIb myosin accounted for around 60% in both *Dnm2*$^{R369W/+}$ and WT mice (Figure 5A). However, a fiber switch occurred toward intermediate type IIa fibers with 25.5% in *Dnm2*$^{R369W/+}$ versus 10.5% in WT

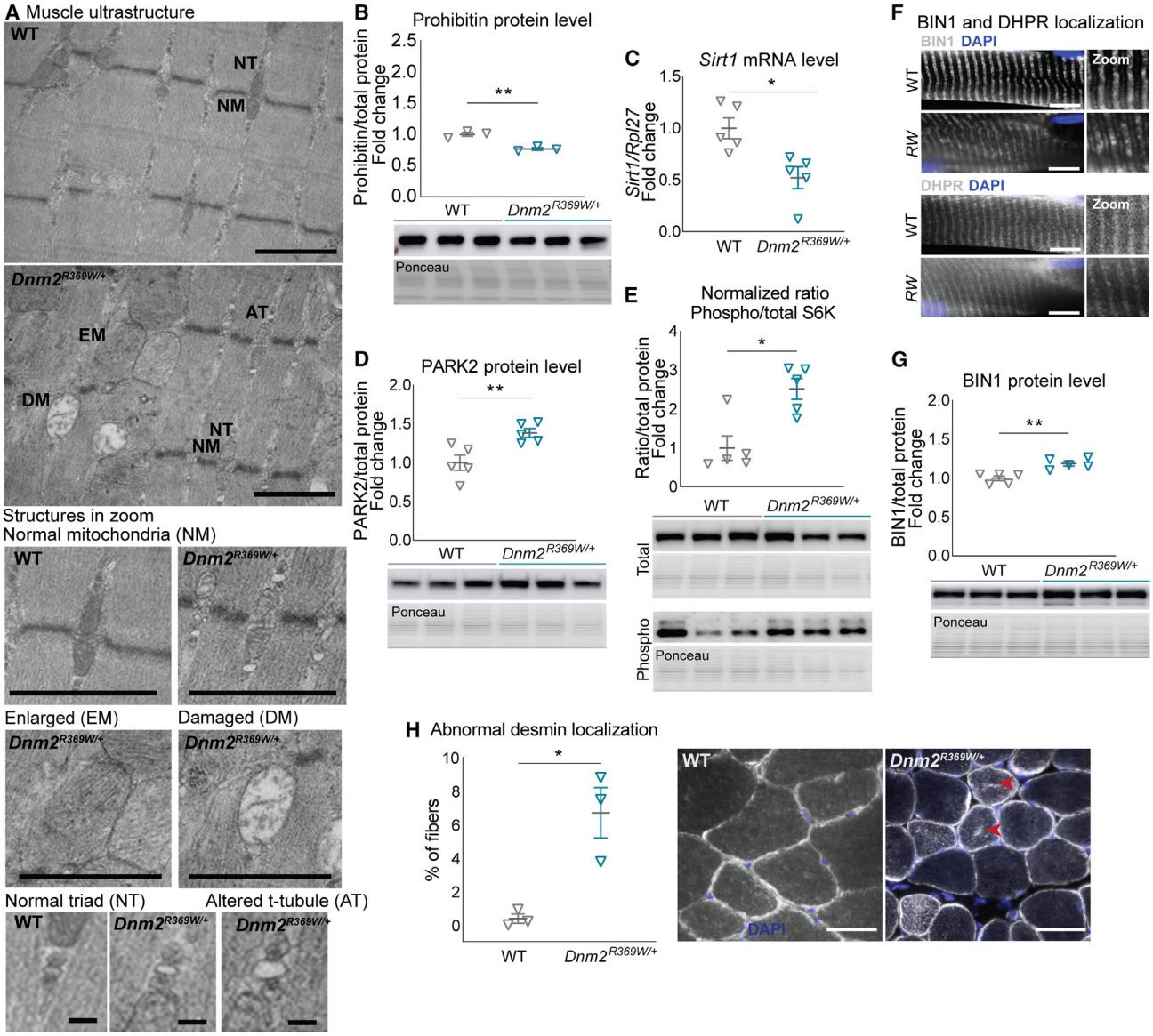

Figure 4. Muscle structure disorganization in *Dnm2*$^{R369W/+}$ mice

(A) Different populations of mitochondria and triads found in electron microscopy: normal mitochondria (NM), enlarged mitochondria (EM), damaged mitochondria (DM, with abnormal cristae), normal triad (NT) and altered T-tubule (AT) (n = 2). Bars in the larger panel and mitochondria represent 1 μm; bars in the triads represent 0.1 μm. (B) Prohibitin protein levels (~30 kDa, n = 3), (C) mRNA level of *Sirt1* and protein levels of (D) PARK2 (~55 kDa, n = 4), and (E) phosphorylated and total S6K (60 kDa, n = 5). (F) BIN1 and DHPR localization in longitudinal muscle sections (n = 3, bar represents 10 μm) and (G) BIN1 protein expression (n = 5, ~60 kDa). (H) Desmin mislocalization (arrows) in transverse muscle sections (n = 3). Mice at 8 weeks old. Bar represents 50 μm. Mean ± SEM. Unpaired t test, *p < 0.05 and **p < 0.01: *Dnm2*$^{R369W/+}$ differs from WT.

muscles. In addition, fibers with negative labeling most probably representing type IIx/d fibers decreased to 15.5% in *Dnm2*$^{R369W/+}$ compared to 29.6% in WT muscles. No type I fibers were found for any genotypes. The mRNA expression of genes coding for the myosin isoforms IIa, IIx/d, and IIb (*MyH7*, *MyH2*, *MyH1*, and *MyH4*) corroborated the immunofluorescence results with overexpression of type IIa (1.36-fold) and downregulation of IIx/d (0.57-fold) corresponding myosin transcripts (Figure 5B). This fiber type profile indicates a significant switch to slower fibers at 8 weeks and a similar tendency at 24 weeks (p = 0.057) (Figure S2). This fiber type switch could explain the force decrease and suggests a trend from a glycolytic toward a more oxidative metabolism in *Dnm2*$^{R369W/+}$ muscles.

To confirm the metabolic switch, we investigated the expression of the muscle isoform of glycogen phosphorylase (PYGM),

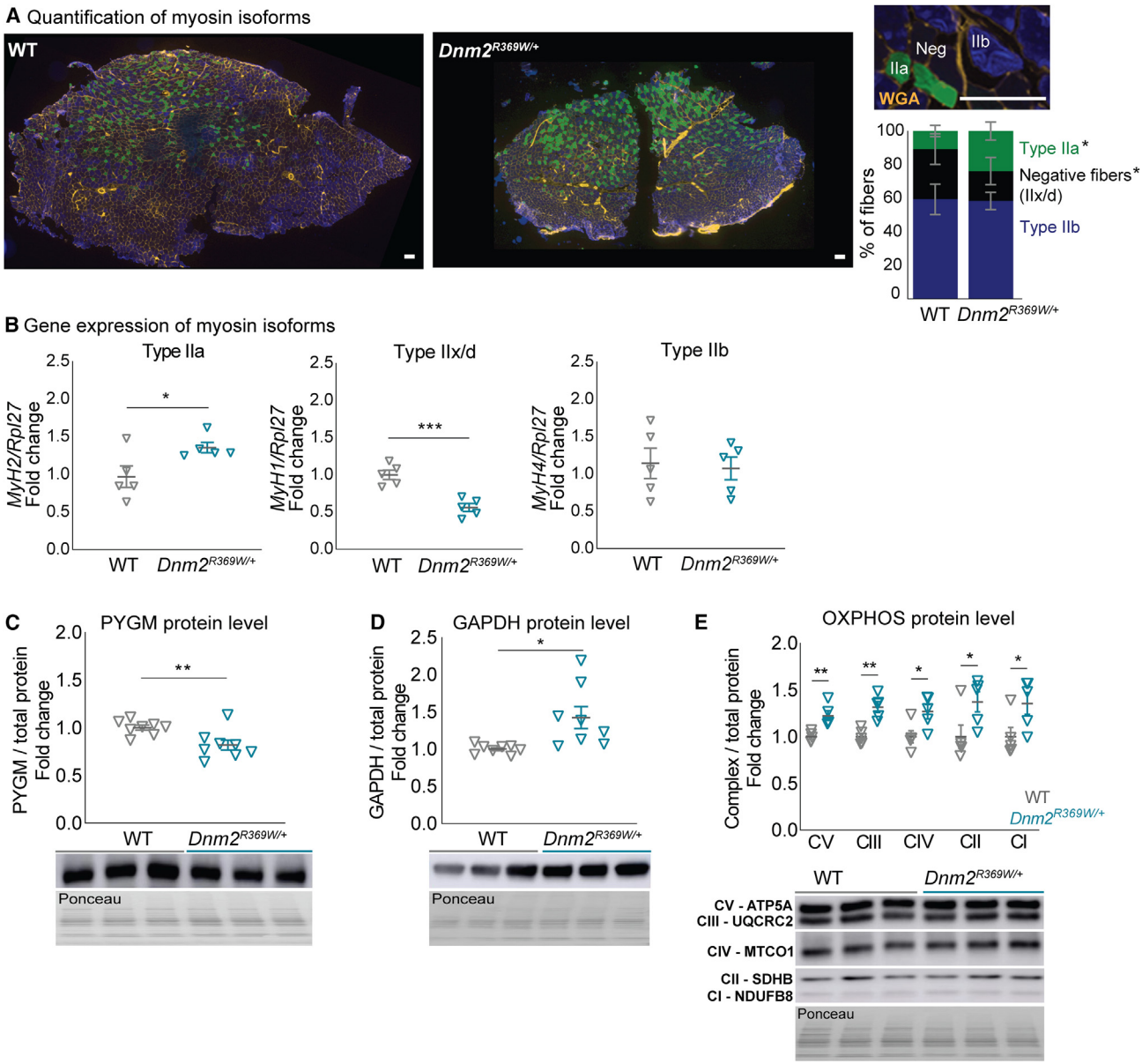

Figure 5. Alterations in muscle fiber metabolism in *Dnm2*$^{R369W/+}$ mice

(A) TA muscle fibers positive for myosin isoforms IIa (MYH2) and IIb (MYH4) per muscle section (total area of 2 mm^2). Negative or light labeling were considered mixed fiber type or type IIx/d. No fiber type I fiber (MYH7) was found. (B) qRT-PCR of genes coding for myosins type IIa, IIx/d, and IIb (*MyH2*, *MyH1*, and *MyH4*, respectively; n = 4) and (C) PYGM (n = 8, ∼100 kDa), (D) GAPDH (n = 8, ∼37 kDa), and (E) OXPHOS (n = 5, ∼15, 25, 35, 40, and 55 kDa) protein levels. Mice at 8 weeks old. Bar represents 100 μm. Mean ± SEM, Mann-Whitney test or unpaired t test: *p < 0.05, **p < 0.01, and ***p < 0.001: *Dnm2*$^{R369W/+}$ differs from WT.

glyceraldehyde-3-phosphate dehydrogenase (GAPDH), and the mitochondrial oxidative phosphorylation system (OXPHOS). PYGM is implicated in energy generation for muscle contraction through glycogenolysis, and GAPDH participates in the sixth step of glycolysis.[53,54] The OXPHOS (mitochondrial complexes I to V) regulates the electron transport chain in the inner mitochondrial membrane for mitochondrial oxidation.[55] The expression of these three markers on western blot was altered in the TA muscles of *Dnm2*$^{R369W/+}$ mice at 8 weeks of age when compared to WT (Figures 5C–5E). PYGM was downregulated (18.2%), GAPDH was upregulated (42.5%), and the quantification of OXPHOS indicated increased expression of all five mitochondrial complexes. These data corroborate with the fiber type switch and support a metabolic alteration toward oxidation in *Dnm2*$^{R369W/+}$ mice.

Normalization of DNM2 levels by sh*Dnm2* injection improved the *Dnm2*$^{R369W/+}$ phenotypes

As we found the CNM-like phenotypes of *Dnm2*$^{R369W/+}$ mice, i.e., muscle hypotrophy with decreased muscle force and altered structural organization of myofibers, correlates with increased level of DNM2 protein, we sought to reduce DNM2 level to improve the disease. sh*Dnm2* targeting the exon 4 of *Dnm2* mRNA was expressed from adeno-associated virus (AAV9) (Figure 1A). One of the TA muscles of *Dnm2*$^{R369W/+}$ mice and WT littermates received a single intramuscular injection of AAV-sh*Dnm2* at 4 weeks old, before reaching mature adulthood.[56] The contralateral TA muscles of the same mice were injected with control AAV-shScramble, which does not hybridize with endogenous *Dnm2* mRNA. The muscles were analyzed at 8 weeks.

The injection of sh*Dnm2* caused downregulation of pan-*Dnm2* by 25% and 27% in the TA muscles of WT and *Dnm2*$^{R369W/+}$ mice, respectively, and the reduction in DNM2 protein expression by 14% in WT and 38% in *Dnm2*$^{R369W/+}$ mice, in comparison to contralateral muscles injected with scramble (Figures 6A and 6B). Importantly, the reduction caused the normalization of *Dnm2* expression in the TA muscles of *Dnm2*$^{R369W/+}$ mice compared to the level of WT scramble. *Dnm2*$^{R369W/+}$ mice injected with sh*Dnm2* displayed normalization of muscle hypotrophy, as indicated by the ratio of muscle to body weight (Figure 6C). The reason for this normalization was the increase in myofiber diameter noted from the (H&E) staining. In particular, there was a significant improvement in the number of large fibers (>40μm minFeret) reaching WT level (Figures 6D and 6E). The aspect of SDH oxidative staining was also improved in *Dnm2*$^{R369W/+}$ mice with the reduction of the number of fibers with abnormal central accumulation of oxidative staining from 14% in scramble to 10.3% in sh*Dnm2* (Figures 6D and 6F). The injection of sh*Dnm2* did not have a noticeable impact in WT muscle (Figure S3).

Normalization of DNM2 levels improved myofiber organization

We observed through electron microscopy that DNM2 normalization by AAV-sh*Dnm2* injection in TA muscles of *Dnm2*$^{R369W/+}$ mice led to some improvements in myofiber organization (Figure 6G). In particular, mitochondria with disrupted cristae were no longer present, albeit there were still some enlarged mitochondria. Concerning the ultrastructure of the triads, they were in normal shape without T-tubules alterations in muscles of *Dnm2*$^{R369W/+}$ mice after sh*Dnm2* injection (Figure 6G). Thus, the improvement of the functional and histological CNM phenotypes of the *Dnm2*$^{R369W/+}$ mice correlated with some improvement in myofiber intracellular organization.

Correlating with the amelioration of the histology and the aspect of the mitochondria and triads in electron microscopy, the absolute force and the specific force of the isolated TA injected with sh*Dnm2* increased by 26% and 16% respectively, compared to the contralateral scramble TA muscles (Figures 6H and 6I). Thus, DNM2 reduction through sh*Dnm2* intramuscular expression improves muscle hypotrophy and force and the CNM-like histopathology of *Dnm2*$^{R369W/+}$ mice. Noteworthy, DNM2 normalization to WT levels is sufficient to achieve this rescue.

DISCUSSION

This study aimed to create, validate, and rescue a mouse model for the moderate form of DNM2-CNM harboring the common *Dnm2* R369W missense mutation and to assess to which extent *Dnm2* targeting is sufficient for a potential therapy. *Dnm2*$^{R369W/+}$ mice presented with increased DNM2 protein level as in patients and moderate CNM-like phenotypes in the TA muscles at 8 weeks, including force deficit, muscle and fiber hypotrophy, and alterations in the myofibers organization including mitochondria with disrupted cristae and some triad structural defects. Normalization of DNM2 levels by AAV-sh*Dnm2* injection targeting *Dnm2* mRNA improved the different phenotypes. These results reveal that the *Dnm2*$^{R369W/+}$ mouse is a faithful model for the moderate form of DNM2-CNM and suggest that DNM2 normalization would be enough to improve the phenotypes in young patients carrying the common *DNM2* R369W mutation.

The *Dnm2*$^{R369W/+}$ mouse is a faithful model for the moderate form of DNM2-CNM

DNM2 R369W patients may manifest a variable number of CNM symptoms at different intensities, such as muscle weakness (proximal, distal, or diffuse) and muscle hypotrophy, with onset ranging from early childhood to early adulthood.[20,23,24] Fiber diameter heterogeneity, mis-localized organelles like nuclei and mitochondria, and altered oxidative stain are histological hallmarks of *DNM2* R369W patients.[12,25] *Dnm2*$^{R369W/+}$ mice reproduce the muscle hypotrophy and decreased muscle force. These defects are obvious in the TA muscle, a muscle especially affected in other mouse models for different genetic forms of CNM.[28,57] DNM2-CNM is described as slowly progressive in patients.[12] Comparative analysis of the *Dnm2*$^{R369W/+}$ phenotypes at 8 and 24 weeks showed worsening of muscle hypotrophy in the TA and GA muscles, and the histology was progressively impacted concerning the number of internalized nuclei and alterations in SDH oxidative stains. A typical and specific oxidative pattern found in DNM2-CNM patients and named “spokes of a wheel” (radial arrangements of sarcoplasmic strands) could also be observed at 24 weeks.

Apart from this new *Dnm2*$^{R369W/+}$ mouse, two other *Dnm2*-CNM mice were characterized and represent models for the mild and severe forms of the disease, respectively *Dnm2*$^{R465W/+}$ and *Dnm2*$^{S619L/+}$. *Dnm2*$^{R465W/+}$ mice present progressive CNM phenotypes including muscle histology disorganization (mainly central accumulation of oxidative stains), muscle and fiber hypotrophy, and compromised muscle contraction.[28,33] TA muscles were affected by hypotrophy at 2 months of age, but the overall histological aspect in H&E staining remained close to normal up to 8 months of age. DNM2 levels were normal at 8 weeks, although contractile properties were impaired at that age. *Dnm2*$^{S619L/+}$ mice present decreased body weight since the very early days postnatal, important impairment in motor function, muscle fiber hypotrophy, abnormal oxidative

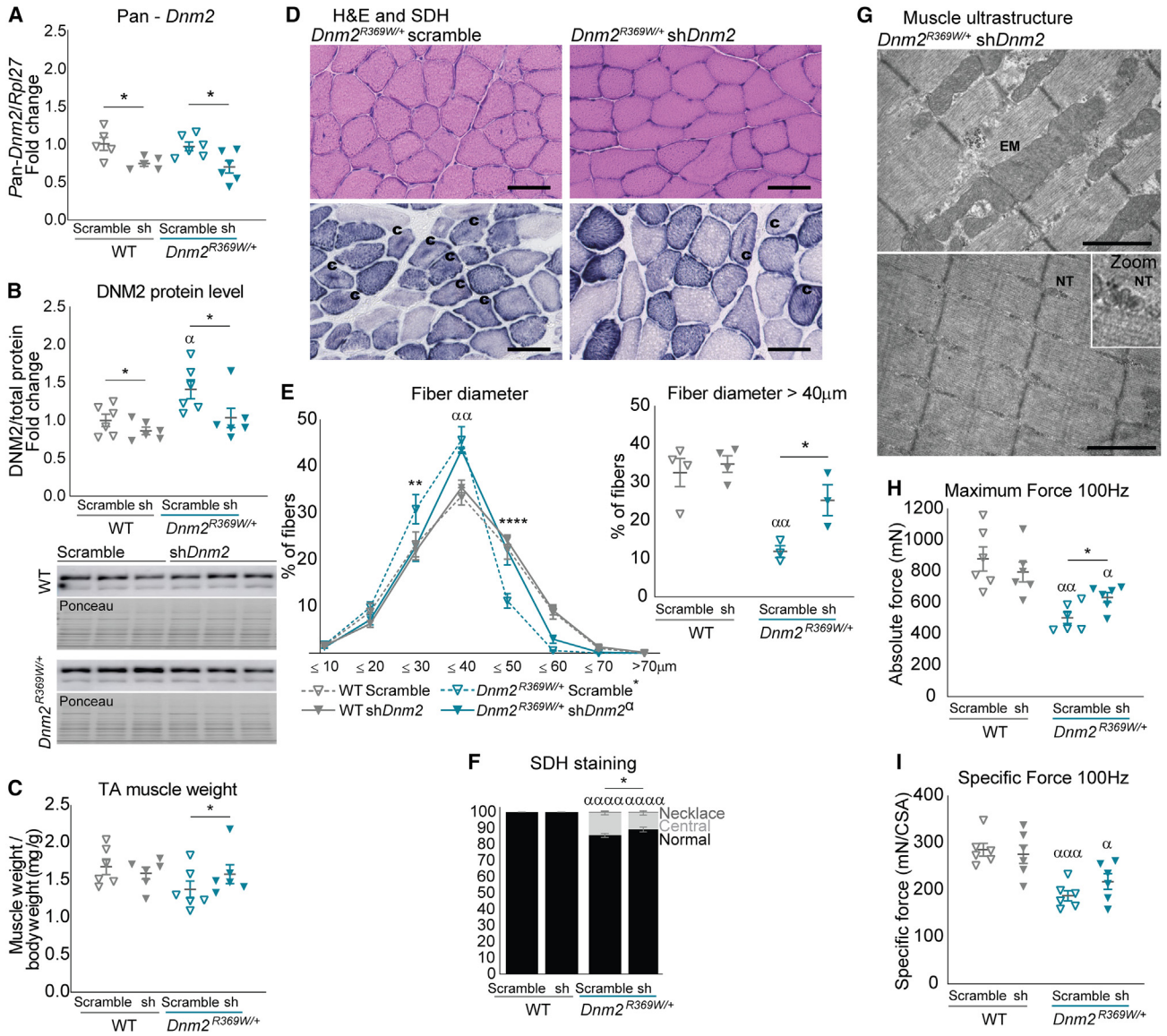

Figure 6. Intramuscular injections of AAV-sh*Dnm2* normalized DNM2 expression, rescued the histopathology, and improved muscle force and ultrastructure

Injections of TA muscles at 4 weeks old, muscles analyzed at 8 weeks old. (A) *Dnm2* mRNA and (B) DNM2 protein expression (n = 5–6). (C) TA muscle weight (n = 6). (D) Transversal muscle sections stained with hematoxylin and eosin and SDH (c: central accumulation) (n = 4). (E) Sections stained with H&E were used to calculate fiber diameter (n = 4). (F) Quantification of SDH staining (n = 3). (G) Electron microscopy of TA muscles from $Dnm2^{R369W/+}$ mice injected with AAV-sh*Dnm2* presenting a mix of enlarged mitochondria (EM) and normal triads (NT) (n = 2). (H) Maximum absolute force and (I) specific force at 100 Hz (n = 6). Mean ± SEM. DNM2 protein level: Wilcoxon matched pairs test, *p < 0.05: $Dnm2^{R369W/+}$ sh*Dnm2* differs from $Dnm2^{R369W/+}$ scramble; Mann-Whitney test, α p < 0.05: $Dnm2^{R369W/+}$ scramble differs from WT scramble. Central staining *p < 0.05: $Dnm2^{R369W/+}$ sh*Dnm2* vs. $Dnm2^{R369W/+}$ scramble; αααα p < 0.0001: $Dnm2^{R369W/+}$ sh*Dnm2* vs. WT sh*Dnm2* or $Dnm2^{R369W/+}$ scramble vs. WT scramble. Others: unpaired t test, α p < 0.05, αα p < 0.01, and ααα p < 0.001: $Dnm2^{R369W/+}$ differs from WT injected with the same treatment; paired t test, *p < 0.05, **p < 0.01, and ****p < 0.0001: scramble vs. sh*Dnm2* within the same genotype.

staining, and enlarged and round-shaped mitochondria with disrupted cristae from 3 weeks of age.[30] Obviously, the phenotype onset and severity of the $Dnm2^{R369W/+}$ mouse are intermediate compared to the $Dnm2^{R465W/+}$ and $Dnm2^{S619L/+}$ mice, indicating the $Dnm2^{R369W/+}$ mouse is a faithful model for the moderate DNM2-CNM form (Figure 7B). Thus, the $Dnm2^{R369W/+}$ mouse is a valuable tool to further decipher the phenotype-genotype correlation, to better understand CNM pathomechanism and disease progression, and to assess if a potential therapy will be applicable to different *DNM2* mutations and CNM severity.

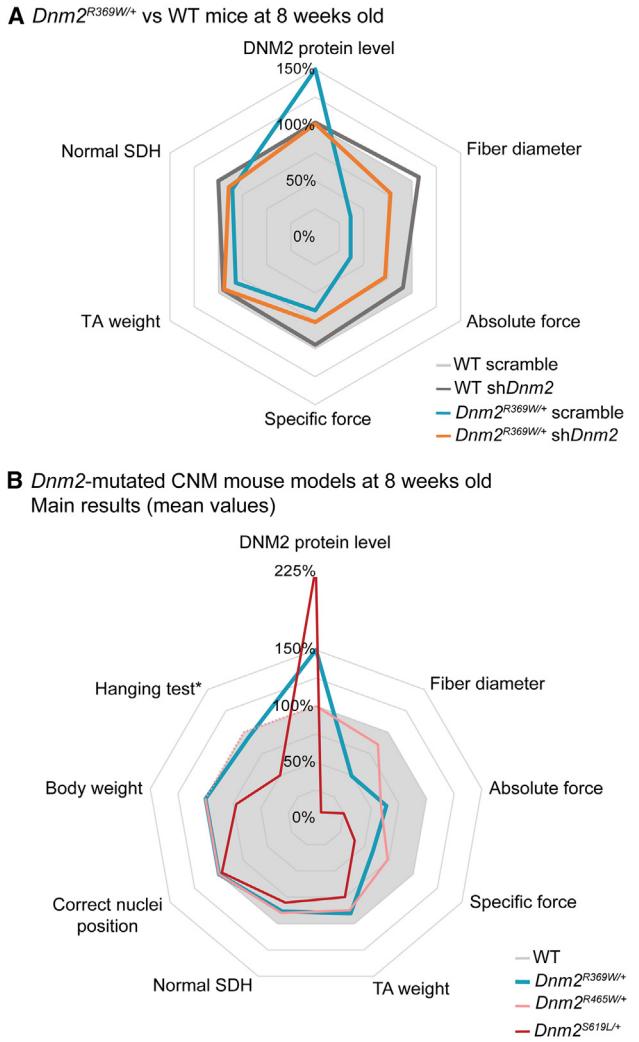

Figure 7. Improvement in CNM-like muscle phenotypes of *Dnm2*$^{R369W/+}$ mice after DNM2 normalization with sh*Dnm2*

(A) Summary of the mean results obtained in WT and *Dnm2*$^{R369W/+}$ mice at 8 weeks old submitted to a single injection of AAV-sh*Dnm2* in the TA muscle and scramble in the contralateral TA at 4 weeks old. 100% represents the normalized values for WT muscles injected with scramble. (B) Mean results obtained for the characterization of *Dnm2*$^{R369W/+}$ mice compared to previously published *Dnm2*-mutated CNM mouse models at 8 weeks old: the severe *Dnm2*$^{S619L/+}$[30] and the mild *Dnm2*$^{R465W/+}$.[28] The data are normalized to the WT values originally reported for each model. *No hanging was test described in the original publication of *Dnm2*$^{R465W/+}$ mice, but it was assumed as equal to the WT. Some of these parameters were not analyzed in (A) as the treatment was intramuscular (for body weight and hanging test) or as centralization of nuclei appeared later than the age of analysis.

Pathological mechanism linked to DNM2-CNM

In patients with DNM2-CNM, the main histopathological hallmarks are organelle mis-positioning and a switch of fiber type toward oxidative metabolism (type I fiber predominance).[58] *Dnm2*$^{R369W/+}$ presented alterations in the expression of myosin isoforms, supporting a switch toward a more oxidative metabolism. Indeed, oxidative or glycolytic fibers correlate with force production: slow oxidative type I fibers are known to produce less force than fast glycolytic type II fibers.[59,60] This difference may be based on the energy production, myosin isoforms, and sensitivity of the contractile apparatus to calcium. Thus, the myosin isoform and metabolic switch discovered in the *Dnm2*$^{R369W/+}$ mouse is a plausible explanation for the force decrease. We cannot exclude additional explanation as alteration of excitation-contraction coupling that was reported in the *Dnm2*$^{R465W/+}$ mouse.[27] The upregulation of the muscle-specific isoform of BIN1 that regulates T-tubule biogenesis and maintenance can potentially represent a compensatory mechanism to such ECC defects. This hypothesis is in accordance with the demonstration that overexpression of BIN1 through transgenesis or AAV transduction improves *Dnm2*$^{R465W/+}$ phenotypes.[61]

Organelles mis-positioning was evidenced in the *Dnm2*$^{R369W/+}$ mouse, and we showed it is progressive with age concerning mitochondria and nuclei. In addition to accumulating toward the central area of the fiber, mitochondria can show enlargement and disrupted cristae. We discovered alteration of upstream and downstream mitophagy markers, strongly supporting that mitochondria defects may be partly caused by defective mitochondrial quality control. It is yet unknown if altered mitophagy is a common finding to several forms of DNM2-CNM as it remains to be tested in the models for the other forms. Of note, we also found internal accumulation of desmin that is found in the *Dnm2*$^{R465W/+}$ mouse and in the MTM1-CNM form,[26,62–64] suggesting general alteration of autophagy is a common pathological mechanism.

Normalization of DNM2 level is sufficient for phenotypic amelioration

DNM2 is overexpressed in patients and mouse models harboring other CNM mutations,[30,57,65] and we confirmed that DNM2 levels were increased in the *Dnm2*$^{R369W/+}$ mice and *DNM2* R369W patients. Local DNM2 reduction was achieved by intramuscular expression of sh*Dnm2* targeting *Dnm2* mRNA through AAV transduction (Figure 7A). A rather short treatment period (4 weeks) was sufficient to achieve both DNM2 normalization to WT level and improvement of the main phenotypes including the muscle hypotrophy, myofiber hypotrophy, and mitochondria mis-position. Similar rescue results were reported for mouse models of the other forms of DNM2-CNM.[30,33] Here we demonstrate that DNM2 normalization is enough to achieve a therapeutic benefit. These data also highlight that a similar treatment could work for different mutations and severity of CNM linked to DNM2.

Concerning the choice of AAV-shRNA instead of siRNA for reducing DNM2 level through RNA interference, the AAV-shRNA approach that was chosen as a single injection was enough to downregulate DNM2 and improve the phenotypes. siRNA has a transient nature that usually requires repeated injections. Moreover, specific and efficient delivery to the tissue of interest is still a major bottleneck. For AAV-shRNA, efficient muscle transduction and long-term expression after several years in human were reported.[66] However, a high

dose of AAV induced liver toxicity in specific disease populations like X-linked CNM.[67] The recent and ongoing development of novel AAV serotype de-targeting the liver and with increased muscle transduction efficiency (thus requiring a lower dose) could help reducing the AAV-shRNA bottlenecks.[68]

MATERIALS AND METHODS

Mice

Dnm2$^{R369W/+}$ C57BL/6N knockin mice (MGI nomenclature *Dnm2*^{em1Ics}) were created by PHENOMIN-Institut Clinique de la Souris (www.phenomin.fr/en-us, Illkirch-Graffenstaden, France) using CRISPR-Cas9 to insert a mutation in the *Dnm2* gene (RefSeq: NM_001039520.2): the CNM-related *R369W* mutations 1293C>T and 1295C>G leading to the substitution Arg – CGC per Trp – TGG, plus a synonym mutation 1292G>A (GAG>GAA) creating an *XmnI* restriction site for genotyping purposes. C57BL/6N fertilized oocytes were microinjected with a mix of sgRNA (TGAGCGCTTT CCCTTTGAAC, 12 ng/μL), spCas9 mRNA (25 g/μL), and single-stranded oligodeoxynucleotides (ssODN, AGATCAAGTAGACACA CTAGAGTTGTCTGGTGGAGCCCGCATCAATCGTATCTTTCA TGAATGGTTTCCCTTTGAACTGGTAAAGGTAGGTGTTCAGC CTGGAGTTAAGTCAGACACTCTCATGCTTGGTCTTTG, 10 ng/μL). The microinjected eggs were re-implanted in CD1 foster females and the germ line transmission was achieved in pups carrying the *XmnI* restriction site and the *R369W* mutation. The mice were genotyped with the primers 5′-CATGCCTCCTTCCAATACACAAAT-3′ and 5′-GAGATCTGGGAAGATGGGGACATGT-3′, and the PCR products were digested with *XmnI* restriction enzyme (20 u/μL) for 30 min at 37°C, followed by electrophoresis and Sanger sequencing.

The mice were housed in the Institut Clinique de la Souris animal facility in 12-h/12-h light/dark cycles, under controlled conditions of temperature and humidity, food and water *ad libitum*. The mice were euthanized by CO_2 inhalation followed by cervical dislocation. All experiments were conducted in accordance with French and European legislations (ethics approval 25185–2020042209385997).

Muscle strength assessment

The hanging test was performed in triplicate by placing the mice horizontally on a grid in suspension, where they were expected to hold against the gravity force for up to 60 s. For the grip test, the mice were weighted, and their force was measured in triplicate using a grip meter (Bioseb Grip Test V3.22, Pinellas Park, FL, USA). The mice were allowed to grab the grip grid and were then gently pulled backward in the horizontal plane. The force obtained was normalized to the body weight.

AAV-sh*Dnm2*

AAV2/9-sh*Dnm2* under the control of a U6 promoter was modified from the sequences created and validated in Buono et al. and Tasfaout et al.[33,56] for the removal of the plasmid region responsible for the GFP expression. The AAV-sh*Dnm2* targeting *Dnm2* exon 4 (sh*Dnm2*, AAGGACATGATCCTGCAGTTCAT, Figure 1A) was injected in the TA muscle. This sequence has 100% homology to the human genome sequence RefSeq: NM_001005360.3.[69] The control AAV-shScramble has no homology to mouse genome (scramble, GGGCTATCCCAACGCTATTAGT) and was injected in the contralateral muscle of 4-week-old-mice at 1.2×10^{10} vg in a final volume of 20 μL. At 8 weeks old, mice were euthanized, and muscles were processed.

Muscle contractile properties

The mice were anesthetized by sequential intraperitoneal injections of Domitor (1 mg/kg)/fentanyl (0.14 mg/kg), diazepam (4 mg/kg), and fentanyl alone (0.14 mg/kg). In sequence, the sciatic nerve was exposed trough a small opening in the gluteus, and the ipsilateral TA muscle was detached and connected to a force transducer Complete1300A mouse Test System (Aurora Scientific, Aurora, Canada). The TA muscle contraction was assessed after sciatic nerve tetanic stimulations at 1, 10, 20, 30, 50, 75, 100 and 150 Hz. The specific force values were obtained by normalizing the absolute force indexes by the cross-sectional area of the muscle analyzed (CSA, TA muscle weight [mg]/TA muscle length [mm] x skeletal muscle density [1.06 mg/mm^3]).[70,71] The fatigue simulation was realized after 3 min of rest by repeated stimulations of TA muscles at 40 Hz (from 1 to 80 pulses).

Tissue processing and histology

The hindlimb muscles were dissected, weighed, snap frozen in liquid nitrogen, cooled in isopentane, and stored at −80°C until processing. Transverse sections of TA muscles (8 μm width) were cut for H&E and SDH stainings and scanned in a NanoZoomer 2HT (Hamamatsu, Iwata, Japan) and processed using ImageJ software (NIH, Bethesda, MD, USA).

Electron microscopy

The TA muscles were fixed in 2.5% glutaraldehyde and 2.5% paraformaldehyde diluted in 0.1 M cacodylate buffer (pH 7.4), washed in cacodylate buffer, postfixed in 1% osmium tetroxide, and dehydrated in ascendant graded alcohol and propylene oxide. The samples were oriented and embedded in Epon 812, sectioned at 70 nm in Ultracut UCT (Leica Biosystems, Wetzlar, Germany) and contrasted with uranyl acetate and lead citrate. In sequence, they were examined at 70 kv with a Morgagni 268D electron microscope (FEI Electron Optics, Eindhoven, Netherlands), and the images were captured using the Mega View III camera (Olympus Soft Imaging Solutions, Tokyo, Japan).

Protein extraction and western blotting

TA muscles from the mice and muscle biopsies from patients (healthy controls: 1 and 2 paraspinal, 3 latissimus dorsi; CNM *DNM2* R369W: 1 deltoid, 2 and 3 vastus lateralis) were lysed in RIPA buffer supplemented with protease inhibitor cocktail EDTA-free (Roche 11873580001, Basel, Switzerland). A total of 10 μg of proteins was applied to SDS-PAGE gels, and the proteins were transferred to nitrocellulose membranes using Trans-blot semi-dry transfer system (Bio-Rad, Hercules, CA, USA). Protein load control was obtained as quantification of Ponceau S staining in the membranes photographed in an Amersham Imager 600 (GE Healthcare Life Sciences, Boston,

MA). The membranes were blocked in 5% milk and incubated with anti-BIN1 (1:20,000, homemade 2405), anti-DNM2 (1:50,000, homemade 2865), anti-GAPDH (1:10,000, Millipore MAB374, Burlington, MA, USA), anti-OXPHOS (1:500, ABCAM ab110413, Cambridge, United Kingdom), anti-PARK2 (1:3,000, Invitrogen, 702785, Waltham, MA, USA), anti-prohibitin (1:1000, ABCAM, ab28172, Cambridge, United Kingdom), anti-PYGM (1:1000, ABCAM ab63158, Cambridge, United Kingdom), anti-total S6K (1:1000, Cell Signaling, 2708, Danvers, MA, USA) or anti-phosphorylated S6K (1:1000, Cell Signaling, 9208, Danvers, MA, USA) and for 1 h with 1:10,000 secondary antibodies conjugated with horseradish. The membranes were exposed to ECL and scanned in an Amersham Imager 600. Blots and total protein (Ponceau S) densities were quantified in ImageJ.

RNA extraction, qRT-PCR, and RT-ddPCR

RNA was extracted from TA muscles with Tri Reagent (Molecular Research Center TR118, Cincinnati, OH, USA) according to the manufacturer's indications, and the cDNA was transcribed using SuperScriptIV Reverse Transcriptase (Thermo Fisher Scientific 18090050, Waltham, MA, USA) and ribonuclease inhibitors (40 U/μL, Promega N2511, Madison, WI, USA). The qRT-PCRs were performed in a LightCycler 480 (Roche, Basel, Switzerland) in triplicate reactions set up with SYBR Green (Qiagen 204145, Hilden, Germany) and *Rpl27*[72] as the housekeeping gene (primers[72–75] in Table S1).

The RT-ddPCR experiments were performed as previously described.[76] In brief, RNA was extracted from the TA muscles of mice at 8 weeks old and transcribed into the cDNA. The RT-ddPCR used FAM or HEX reporter dyes and ZEN/Iowa Black FQ double-quenched nuclease probes (IDT, Coralville, IA, USA) either targeting the 5′ region of WT or mutated form of *Dnm2*. The reactions were conducted in a QX200 Droplet Digital PCR System (Bio-Rad, Hercules, CA, USA), and the *Hprt* gene was used for housekeeping (Table S2).

Immunofluorescence

For immunofluorescence, TA muscles from mice were used. Longitudinal sections of TA muscles were fixed in PFA 4% overnight, cryopreserved in sucrose 30% and sectioned in cryostat. Transverse sections were fixed in PFA 4% prior to the immunofluorescence reactions. The samples were permeabilized with Triton 0.2% and blocked in 5% BSA. The slides were incubated with 1:100 of anti-α actinin (Sigma-Aldrich A7811, St. Louis, MO, USA), anti-BIN1 IgG2 (Sigma-Aldrich B9428, St. Louis, MO, USA), anti-desmin (ABCAM AB15200, Cambridge, United Kingdom), anti-DHPR IgG1 (ABCAM ab2862, Cambridge, United Kingdom), anti-DNM2 (homemade 2680) or anti-PAX7 (Developmental Studies Hybridoma Bank PAX7, Iowa, IA, USA), and 1:250 of the suitable fluorescent secondary antibody plus 1:1,000 DAPI for 1 h 30 min at room temperature.

The fiber type immunofluorescence was performed in non-fixed and non-permeabilized transverse muscle sections. The samples were blocked in 3% BSA and incubated with a mix of the primary antibodies 1:50 anti-myosin type I, MYH7 (Developmental Studies Hybridoma Bank BA-D5, IgG2b, Iowa, IA, USA), 1:50 anti-myosin type IIa, MYH2 (Developmental Studies Hybridoma Bank SC-71, IgG1, Iowa, IA, USA), and 1:50 anti-myosin type IIb, MYH4 (Developmental Studies Hybridoma Bank BF-F3, IgM, Iowa, IA, USA). Next, the samples were incubated with a mix of the secondary antibodies 1:100 anti-IgG2b Cy3 dye (Jackson ImmunoResearch 115-165-207 West Grove, PA, USA), 1:100 anti-IgG1 Alexa Fluor 488 dye (Jackson ImmunoResearch 115-545-205 West Grove, PA, USA), 1:100 anti-IgM DyLight 405 dye (Jackson ImmunoResearch 115-475-075 West Grove, PA, USA), plus 1:200 wheat germ agglutinin Alexa Fluor 647 dye (Invitrogen W32466, Waltham, MA, USA).

Statistics

Statistical analyses were performed in the GraphPad Prism 8 software (GraphPad, San Diego, CA, USA). After the determination of samples distribution profile by Shapiro-Wilk test, the appropriate statistic test was performed as indicated in the figure legends. Significant variations were accepted when $p < 0.05$.

Study approval

All experiments were conducted in accordance with French and European legislations and approved by the institutional ethics committee (project number 25185–2020042209385997 and CE-2022-3).

DATA AND CODE AVAILABILITY

The authors confirm that the data supporting the findings of this study are available within the article and/or its supplemental material.

SUPPLEMENTAL INFORMATION

Supplemental information can be found online at https://doi.org/10.1016/j.omtn.2023.07.003.

ACKNOWLEDGMENTS

The authors would like to thank the scientific platforms at the Institut de Génétique et de Biologie Moléculaire et Cellulaire (IGBMC) and Institut Clinique de la Souris (ICS), mainly Nadia Messaddeq for the electron microscopy preparation and images, Pascale Koebel for producing the plasmids used in this study, Loic Lindner and Pauline Cayrou for the RT-ddPCR reactions, the PHENOMIN-ICS for the establishment of the *Dnm2* mouse mutant line, and Dr Karlin Boujman, Dr Nicol C. Voermans (Donders Institute for Brain, Cognition and Behavior, Radboud University Medical Center, Netherlands), Dr Stephane Vasseur (Myobank-AFM, Institut de Myologie, France), and Dr Yvan De Feraudy (Médecine translationnelle et neurogénétique, IGBMC, France) for the human samples. The graphical abstract was created with BioRender.com. This work is part of the Interdisciplinary Thematic Institute IMCBio, as part of the ITI 2021–2028 program of the University of Strasbourg, CNRS and Inserm, and was supported by IdEx Unistra (ANR-10-IDEX-0002) and by SFRI-STRAT'US project (ANR 20-SFRI-0012) and EUR IMCBio (ANR-17-EURE-0023) under the framework of the French Investments for the Future Program. This work was also supported by a donation from Roland Sackers.

AUTHOR CONTRIBUTIONS

J.C.N. and J.L. conceived the project and analyzed the data. J.C.N. and F.M.F. performed experiments. J.C.N. and J.L. wrote the manuscript. J.B. and J.L. provided funding. J.L. supervised the work.

DECLARATION OF INTERESTS

J.L. is co-founder of Dynacure.

REFERENCES

1. Gold, E.S., Underhill, D.M., Morrissette, N.S., Guo, J., McNiven, M.A., and Aderem, A. (1999). Dynamin 2 is required for phagocytosis in macrophages. J. Exp. Med. *190*, 1849–1856.
2. Kruchten, A.E., and McNiven, M.A. (2006). Dynamin as a mover and pincher during cell migration and invasion. J. Cell Sci. *119*, 1683–1690.
3. Praefcke, G.J.K., and McMahon, H.T. (2004). The dynamin superfamily: universal membrane tubulation and fission molecules? Nat. Rev. Mol. Cell Biol. *5*, 133–147.
4. Ferguson, S.M., and De Camilli, P. (2012). Dynamin, a membrane-remodelling GTPase. Nat. Rev. Mol. Cell Biol. *13*, 75–88.
5. Chappie, J.S., Acharya, S., Liu, Y.W., Leonard, M., Pucadyil, T.J., and Schmid, S.L. (2009). An intramolecular signaling element that modulates dynamin function in vitro and in vivo. Mol. Biol. Cell *20*, 3561–3571.
6. Faelber, K., Posor, Y., Gao, S., Held, M., Roske, Y., Schulze, D., Haucke, V., Noé, F., and Daumke, O. (2011). Crystal structure of nucleotide-free dynamin. Nature *477*, 556–560.
7. Jimah, J.R., and Hinshaw, J.E. (2019). Structural Insights into the Mechanism of Dynamin Superfamily Proteins. Trends Cell Biol. *29*, 257–273.
8. Klein, D.E., Lee, A., Frank, D.W., Marks, M.S., and Lemmon, M.A. (1998). The pleckstrin homology domains of dynamin isoforms require oligomerization for high affinity phosphoinositide binding. J. Biol. Chem. *273*, 27725–27733.
9. Srinivasan, S., Dharmarajan, V., Reed, D.K., Griffin, P.R., and Schmid, S.L. (2016). Identification and function of conformational dynamics in the multidomain GTPase dynamin. EMBO J. *35*, 443–457.
10. McNiven, M.A., Cao, H., Pitts, K.R., and Yoon, Y. (2000). The dynamin family of mechanoenzymes: pinching in new places. Trends Biochem. Sci. *25*, 115–120.
11. Cowling, B.S., Prokic, I., Tasfaout, H., Rabai, A., Humbert, F., Rinaldi, B., Nicot, A.S., Kretz, C., Friant, S., Roux, A., and Laporte, J. (2017). Amphiphysin (BIN1) negatively regulates dynamin 2 for normal muscle maturation. J. Clin. Invest. *127*, 4477–4487.
12. Bitoun, M., Maugenre, S., Jeannet, P.Y., Lacène, E., Ferrer, X., Laforêt, P., Martin, J.J., Laporte, J., Lochmüller, H., Beggs, A.H., et al. (2005). Mutations in dynamin 2 cause dominant centronuclear myopathy. Nat. Genet. *37*, 1207–1209.
13. Kenniston, J.A., and Lemmon, M.A. (2010). Dynamin GTPase regulation is altered by PH domain mutations found in centronuclear myopathy patients. EMBO J. *29*, 3054–3067.
14. Chin, Y.H., Lee, A., Kan, H.W., Laiman, J., Chuang, M.C., Hsieh, S.T., and Liu, Y.W. (2015). Dynamin-2 mutations associated with centronuclear myopathy are hypermorphic and lead to T-tubule fragmentation. Hum. Mol. Genet. *24*, 5542–5554.
15. Wang, L., Barylko, B., Byers, C., Ross, J.A., Jameson, D.M., and Albanesi, J.P. (2010). Dynamin 2 mutants linked to centronuclear myopathies form abnormally stable polymers. J. Biol. Chem. *285*, 22753–22757.
16. Cowling, B.S., Toussaint, A., Amoasii, L., Koebel, P., Ferry, A., Davignon, L., Nishino, I., Mandel, J.L., and Laporte, J. (2011). Increased expression of wild-type or a centronuclear myopathy mutant of dynamin 2 in skeletal muscle of adult mice leads to structural defects and muscle weakness. Am. J. Pathol. *178*, 2224–2235.
17. Liu, N., Bezprozvannaya, S., Shelton, J.M., Frisard, M.I., Hulver, M.W., McMillan, R.P., Wu, Y., Voelker, K.A., Grange, R.W., Richardson, J.A., et al. (2011). Mice lacking microRNA 133a develop dynamin 2-dependent centronuclear myopathy. J. Clin. Invest. *121*, 3258–3268.
18. Bitoun, M., Bevilacqua, J.A., Eymard, B., Prudhon, B., Fardeau, M., Guicheney, P., and Romero, N.B. (2009). A new centronuclear myopathy phenotype due to a novel dynamin 2 mutation. Neurology *72*, 93–95.
19. Bitoun, M., Bevilacqua, J.A., Prudhon, B., Maugenre, S., Taratuto, A.L., Monges, S., Lubieniecki, F., Cances, C., Uro-Coste, E., Mayer, M., et al. (2007). Dynamin 2 mutations cause sporadic centronuclear myopathy with neonatal onset. Ann. Neurol. *62*, 666–670.
20. Böhm, J., Biancalana, V., Dechene, E.T., Bitoun, M., Pierson, C.R., Schaefer, E., Karasoy, H., Dempsey, M.A., Klein, F., Dondaine, N., et al. (2012). Mutation spectrum in the large GTPase dynamin 2, and genotype-phenotype correlation in autosomal dominant centronuclear myopathy. Hum. Mutat. *33*, 949–959.
21. Biancalana, V., Romero, N.B., Thuestad, I.J., Ignatius, J., Kataja, J., Gardberg, M., Héron, D., Malfatti, E., Oldfors, A., and Laporte, J. (2018). Some DNM2 mutations cause extremely severe congenital myopathy and phenocopy myotubular myopathy. Acta Neuropathol. Commun. *6*, 93.
22. Abath Neto, O., Martins, C.d.A., Carvalho, M., Chadi, G., Seitz, K.W., Oliveira, A.S.B., Reed, U.C., Laporte, J., and Zanoteli, E. (2015). DNM2 mutations in a cohort of sporadic patients with centronuclear myopathy. Genet. Mol. Biol. *38*, 147–151.
23. Fattori, F., Maggi, L., Bruno, C., Cassandrini, D., Codemo, V., Catteruccia, M., Tasca, G., Berardinelli, A., Magri, F., Pane, M., et al. (2015). Centronuclear myopathies: genotype-phenotype correlation and frequency of defined genetic forms in an Italian cohort. J. Neurol. *262*, 1728–1740.
24. Mori-Yoshimura, M., Okuma, A., Oya, Y., Fujimura-Kiyono, C., Nakajima, H., Matsuura, K., Takemura, A., Malicdan, M.C.V., Hayashi, Y.K., Nonaka, I., et al. (2012). Clinicopathological features of centronuclear myopathy in Japanese populations harboring mutations in dynamin 2. Clin. Neurol. Neurosurg. *114*, 678–683.
25. Romero, N.B. (2010). Centronuclear myopathies: a widening concept. Neuromuscul. Disord. *20*, 223–228.
26. Puri, C., Manni, M.M., Vicinanza, M., Hilcenko, C., Zhu, Y., Runwal, G., Stamatakou, E., Menzies, F.M., Mamchaoui, K., Bitoun, M., and Rubinsztein, D.C. (2020). A DNM2 Centronuclear Myopathy Mutation Reveals a Link between Recycling Endosome Scission and Autophagy. Dev. Cell *53*, 154–168.e6.
27. Kutchukian, C., Szentesi, P., Allard, B., Trochet, D., Beuvin, M., Berthier, C., Tourneur, Y., Guicheney, P., Csernoch, L., Bitoun, M., and Jacquemond, V. (2017). Impaired excitation-contraction coupling in muscle fibres from the dynamin2(R465W) mouse model of centronuclear myopathy. J. Physiol. *595*, 7369–7382.
28. Durieux, A.C., Vignaud, A., Prudhon, B., Viou, M.T., Beuvin, M., Vassilopoulos, S., Fraysse, B., Ferry, A., Lainé, J., Romero, N.B., et al. (2010). A centronuclear myopathy-dynamin 2 mutation impairs skeletal muscle structure and function in mice. Hum. Mol. Genet. *19*, 4820–4836.
29. Zhao, M., Smith, L., Volpatti, J., Fabian, L., and Dowling, J.J. (2019). Insights into wild type dynamin 2 and the consequences of DNM2 mutations from transgenic zebrafish. Hum. Mol. Genet. *28*, 4186–4196.
30. Massana Muñoz, X., Kretz, C., Silva-Rojas, R., Ochala, J., Menuet, A., Romero, N.B., Cowling, B.S., and Laporte, J. (2020). Physiological impact and disease reversion for the severe form of centronuclear myopathy linked to dynamin. JCI Insight *5*, e137899.
31. Dowling, J.J., Joubert, R., Low, S.E., Durban, A.N., Messaddeq, N., Li, X., Dulin-Smith, A.N., Snyder, A.D., Marshall, M.L., Marshall, J.T., et al. (2012). Myotubular myopathy and the neuromuscular junction: a novel therapeutic approach from mouse models. Dis. Model. Mech. *5*, 852–859.
32. Robb, S.A., Sewry, C.A., Dowling, J.J., Feng, L., Cullup, T., Lillis, S., Abbs, S., Lees, M.M., Laporte, J., Manzur, A.Y., et al. (2011). Impaired neuromuscular transmission and response to acetylcholinesterase inhibitors in centronuclear myopathies. Neuromuscul. Disord. *21*, 379–386.
33. Buono, S., Ross, J.A., Tasfaout, H., Levy, Y., Kretz, C., Tayefeh, L., Matson, J., Guo, S., Kessler, P., et al. (2018). Reducing dynamin 2 (DNM2) rescues DNM2-related dominant centronuclear myopathy. Proc. Natl. Acad. Sci. USA *115*, 11066–11071.
34. Trochet, D., Prudhon, B., Beuvin, M., Peccate, C., Lorain, S., Julien, L., Benkhelifa-Ziyyat, S., Rabai, A., Mamchaoui, K., Ferry, A., et al. (2018). Allele-specific silencing therapy for Dynamin 2-related dominant centronuclear myopathy. EMBO Mol. Med. *10*, 239–253.
35. Dudhal, S., Mekzine, L., Prudhon, B., Soocheta, K., Cadot, B., Mamchaoui, K., Trochet, D., and Bitoun, M. (2022). Development of versatile allele-specific siRNAs able to silence all the dominant dynamin 2 mutations. Mol. Ther. Nucleic Acids *29*, 733–748.
36. Nijtmans, L.G., de Jong, L., Artal Sanz, M., Coates, P.J., Berden, J.A., Back, J.W., Muijsers, A.O., van der Spek, H., and Grivell, L.A. (2000). Prohibitins act as a

membrane-bound chaperone for the stabilization of mitochondrial proteins. EMBO J. *19*, 2444–2451.

37. Harper, J.W., Ordureau, A., and Heo, J.M. (2018). Building and decoding ubiquitin chains for mitophagy. Nat. Rev. Mol. Cell Biol. *19*, 93–108.

38. Pickles, S., Vigié, P., and Youle, R.J. (2018). Mitophagy and Quality Control Mechanisms in Mitochondrial Maintenance. Curr. Biol. *28*, R170–R185.

39. Matsuda, N., Sato, S., Shiba, K., Okatsu, K., Saisho, K., Gautier, C.A., Sou, Y.S., Saiki, S., Kawajiri, S., Sato, F., et al. (2010). PINK1 stabilized by mitochondrial depolarization recruits Parkin to damaged mitochondria and activates latent Parkin for mitophagy. J. Cell Biol. *189*, 211–221.

40. Wan, W., Hua, F., Fang, P., Li, C., Deng, F., Chen, S., Ying, J., and Wang, X. (2022). Regulation of Mitophagy by Sirtuin Family Proteins: A Vital Role in Aging and Age-Related Diseases. Front. Aging Neurosci. *14*, 845330.

41. Tran, Q., Jung, J.H., Park, J., Lee, H., Hong, Y., Cho, H., Kim, M., Park, S., Kwon, S.H., Kim, S.H., et al. (2018). S6 kinase 1 plays a key role in mitochondrial morphology and cellular energy flow. Cell. Signal. *48*, 13–24.

42. Saxton, R.A., and Sabatini, D.M. (2017). mTOR Signaling in Growth, Metabolism, and Disease. Cell *169*, 361–371.

43. Shishmarev, D. (2020). Excitation-contraction coupling in skeletal muscle: recent progress and unanswered questions. Biophys. Rev. *12*, 143–153.

44. Curtis, B.M., and Catterall, W.A. (1984). Purification of the calcium antagonist receptor of the voltage-sensitive calcium channel from skeletal muscle transverse tubules. Biochemistry *23*, 2113–2118.

45. Fosset, M., Jaimovich, E., Delpont, E., and Lazdunski, M. (1983). [3H]nitrendipine receptors in skeletal muscle. J. Biol. Chem. *258*, 6086–6092.

46. Lee, E., Marcucci, M., Daniell, L., Pypaert, M., Weisz, O.A., Ochoa, G.C., Farsad, K., Wenk, M.R., and De Camilli, P. (2002). Amphiphysin 2 (Bin1) and T-tubule biogenesis in muscle. Science *297*, 1193–1196.

47. Razzaq, A., Robinson, I.M., McMahon, H.T., Skepper, J.N., Su, Y., Zelhof, A.C., Jackson, A.P., Gay, N.J., and O'Kane, C.J. (2001). Amphiphysin is necessary for organization of the excitation-contraction coupling machinery of muscles, but not for synaptic vesicle endocytosis in Drosophila. Genes Dev. *15*, 2967–2979.

48. Agnetti, G., Herrmann, H., and Cohen, S. (2022). New roles for desmin in the maintenance of muscle homeostasis. FEBS J. *289*, 2755–2770.

49. Roman, W., Martins, J.P., Carvalho, F.A., Voituriez, R., Abella, J.V.G., Santos, N.C., Cadot, B., Way, M., and Gomes, E.R. (2017). Myofibril contraction and crosslinking drive nuclear movement to the periphery of skeletal muscle. Nat. Cell Biol. *19*, 1189–1201.

50. Fongy, A., Falcone, S., Lainé, J., Prudhon, B., Martins-Bach, A., and Bitoun, M. (2019). Nuclear defects in skeletal muscle from a Dynamin 2-linked centronuclear myopathy mouse model. Sci. Rep. *9*, 1580.

51. Augusto, V., Padovani, C.R., and Campos, G.E.R. (2004). Skeletal muscle fiber types in C57BL6J mice. Journal of Morphological Sciences *21*, 89–94.

52. Kammoun, M., Cassar-Malek, I., Meunier, B., and Picard, B. (2014). A simplified immunohistochemical classification of skeletal muscle fibres in mouse. Eur. J. Histochem. *58*, 2254.

53. Llavero, F., Arrazola Sastre, A., Luque Montoro, M., Gálvez, P., Lacerda, H.M., Parada, L.A., and Zugaza, J.L. (2019). McArdle Disease: New Insights into Its Underlying Molecular Mechanisms. Int. J. Mol. Sci. *20*, 5919.

54. Song, S., and Finkel, T. (2007). GAPDH and the search for alternative energy. Nat. Cell Biol. *9*, 869–870.

55. Fernandez-Vizarra, E., and Zeviani, M. (2021). Mitochondrial disorders of the OXPHOS system. FEBS Lett. *595*, 1062–1106.

56. Tasfaout, H., Lionello, V.M., Kretz, C., Koebel, P., Messaddeq, N., Bitz, D., Laporte, J., and Cowling, B.S. (2018). Single Intramuscular Injection of AAV-shRNA Reduces DNM2 and Prevents Myotubular Myopathy in Mice. Mol. Ther. *26*, 1082–1092.

57. Cowling, B.S., Chevremont, T., Prokic, I., Kretz, C., Ferry, A., Coirault, C., Koutsopoulos, O., Laugel, V., Romero, N.B., and Laporte, J. (2014). Reducing dynamin 2 expression rescues X-linked centronuclear myopathy. J. Clin. Invest. *124*, 1350–1363.

58. Fischer, D., Herasse, M., Bitoun, M., Barragán-Campos, H.M., Chiras, J., Laforêt, P., Fardeau, M., Eymard, B., Guicheney, P., and Romero, N.B. (2006). Characterization of the muscle involvement in dynamin 2-related centronuclear myopathy. Brain *129*, 1463–1469.

59. Schiaffino, S., and Reggiani, C. (2011). Fiber types in mammalian skeletal muscles. Physiol. Rev. *91*, 1447–1531.

60. Frontera, W.R., and Ochala, J. (2015). Skeletal muscle: a brief review of structure and function. Calcif. Tissue Int. *96*, 183–195.

61. Lionello, V.M., Kretz, C., Edelweiss, E., Crucifix, C., Gómez-Oca, R., Messaddeq, N., Buono, S., Koebel, P., Massana Muñoz, X., Diedhiou, N., et al. (2022). BIN1 modulation in vivo rescues dynamin-related myopathy. Proc. Natl. Acad. Sci. USA *119*, e2109576119.

62. Durieux, A.C., Vassilopoulos, S., Lainé, J., Fraysse, B., Briñas, L., Prudhon, B., Castells, J., Freyssenet, D., Bonne, G., Guicheney, P., and Bitoun, M. (2012). A centronuclear myopathy–dynamin 2 mutation impairs autophagy in mice. Traffic *13*, 869–879.

63. Al-Qusairi, L., Prokic, I., Amoasii, L., Kretz, C., Messaddeq, N., Mandel, J.L., and Laporte, J. (2013). Lack of myotubularin (MTM1) leads to muscle hypotrophy through unbalanced regulation of the autophagy and ubiquitin-proteasome pathways. Faseb. J. *27*, 3384–3394.

64. Hnia, K., Tronchère, H., Tomczak, K.K., Amoasii, L., Schultz, P., Beggs, A.H., Payrastre, B., Mandel, J.L., and Laporte, J. (2011). Myotubularin controls desmin intermediate filament architecture and mitochondrial dynamics in human and mouse skeletal muscle. J. Clin. Invest. *121*, 70–85.

65. Toussaint, A., Cowling, B.S., Hnia, K., Mohr, M., Oldfors, A., Schwab, Y., Yis, U., Maisonobe, T., Stojkovic, T., Wallgren-Pettersson, C., et al. (2011). Defects in amphiphysin 2 (BIN1) and triads in several forms of centronuclear myopathies. Acta Neuropathol. *121*, 253–266.

66. Mendell, J.R., Al-Zaidy, S.A., Rodino-Klapac, L.R., Goodspeed, K., Gray, S.J., Kay, C.N., Boye, S.L., Boye, S.E., George, L.A., Salabarria, S., et al. (2021). Current Clinical Applications of In Vivo Gene Therapy with AAVs. Mol. Ther. *29*, 464–488.

67. Kishimoto, T.K., and Samulski, R.J. (2022). Addressing high dose AAV toxicity - 'one and done' or 'slower and lower. Expet Opin. Biol. Ther. *22*, 1067–1071.

68. Tabebordbar, M., Lagerborg, K.A., Stanton, A., King, E.M., Ye, S., Tellez, L., Krunnfusz, A., Tavakoli, S., Widrick, J.J., Messemer, K.A., et al. (2021). Directed evolution of a family of AAV capsid variants enabling potent muscle-directed gene delivery across species. Cell *184*, 4919–4938.e22.

69. (1988). Nucleotide (National Center for Biotechnology Information). https://www.ncbi.nlm.nih.gov/nucleotide/.

70. Brooks, S.V., and Faulkner, J.A. (1988). Contractile properties of skeletal muscles from young, adult and aged mice. J. Physiol. *404*, 71–82.

71. Distefano, G., Ferrari, R.J., Weiss, C., Deasy, B.M., Boninger, M.L., Fitzgerald, G.K., Huard, J., and Ambrosio, F. (2013). Neuromuscular electrical stimulation as a method to maximize the beneficial effects of muscle stem cells transplanted into dystrophic skeletal muscle. PLoS One *8*, e54922.

72. Thomas, K.C., Zheng, X.F., Garces Suarez, F., Raftery, J.M., Quinlan, K.G.R., Yang, N., North, K.N., and Houweling, P.J. (2014). Evidence based selection of commonly used RT-qPCR reference genes for the analysis of mouse skeletal muscle. PLoS One *9*, e88653.

73. Honda, M., Hidaka, K., Fukada, S.I., Sugawa, R., Shirai, M., Ikawa, M., and Morisaki, T. (2017). Vestigial-like 2 contributes to normal muscle fiber type distribution in mice. Sci. Rep. *7*, 7168.

74. Gómez-Oca, R., Edelweiss, E., Djeddi, S., Gerbier, M., Massana-Muñoz, X., Oulad-Abdelghani, M., Crucifix, C., Spiegelhalter, C., Messaddeq, N., Poussin-Courmontagne, P., et al. (2022). Differential impact of ubiquitous and muscle dynamin 2 isoforms in muscle physiology and centronuclear myopathy. Nat. Commun. *13*, 6849.

75. Luo, H., Zhou, M., Ji, K., Zhuang, J., Dang, W., Fu, S., Sun, T., and Zhang, X. (2017). Expression of Sirtuins in the Retinal Neurons of Mice, Rats, and Humans. Front. Aging Neurosci. *9*, 366.

76. Lindner, L., Cayrou, P., Jacquot, S., Birling, M.C., Herault, Y., and Pavlovic, G. (2021). Reliable and robust droplet digital PCR (ddPCR) and RT-ddPCR protocols for mouse studies. Methods *191*, 95–106.